Review paper: The 14th October 1968 M_w 6.6 Meckering surface rupturing earthquake, Australia

Tamarah King

School of Earth Sciences, The University of Melbourne, Victoria 3010, Australia
tamarah.king@unimelb.edu.au
https://orcid.org/0000-0002-9654-2917

Mark Quigley

School of Earth Sciences, The University of Melbourne, Victoria 3010, Australia
Mark.quigley@unimelb.edu.au
https://orcid.org/0000-0002-4430-4212

Dan Clark

Geoscience Australia, Canberra 2601, Australia
https://orcid.org/0000-0001-5387-4404

Abstract

The 14th October 1968 M_W 6.6 Meckering earthquake surface rupture is comprised of a main 37 km long concave Meckering scarp (with a 1.5 km wide dextral step-over along the Burges en-echelon rupture complex) and a minor 9 km long rupture on the Meckering scarp foot-wall (the Splinter scarp, also with a 1.5 km dextral step-over). We recommend a total surface rupture length of 44.4 km for implementation into magnitude-length scaling relationships based on a reassessment of primary rupture lengths. High resolution aeromagnetic data show the arcuate limbs of the Meckering scarp are controlled by basement structures, with supportive evidence from surface outcrops. No definitive evidence exists to support any rupture along these structures between their Archean - Proterozoic formation and Tertiary to Quaternary sedimentation. The rupture is characterised by near-surface bedrock along most of its length, and available trenching shows only the historical offsets. We find that available seismological, geological and surface rupture data support a model in which rupture intiates on the Splinter fault as a sub-event 3.5 sec before the mainshock, propagating to the surface and downwards to an intersection with the main Meckering fault at 2.8 km depth (consistent with centroid depth estimates of 2.3 – 3.0 km). Rupture then propagates bi-laterally from the fault intersection across the Meckering faults to produce the mainshock. Further modelling would be required to test the strength of this model. This earthquake is one of the most structurally complex (as proxied by the number of discrete faults) for its magnitude, as evidenced by comparison with a global compilation.

This document presents a review of available literature related to the 1968 Meckering surface rupturing earthquake. It includes newly digitised data related to the rupture and new interpretations of controls on fault rupture. It supplements a manuscript reviewing all Australian surface rupturing earthquakes, submitted to Geosciences in August 2019.

Please contact authors on the content presented herein; we welcome constructive feedback.

---

1. Geology

1.1 Regional

The 1968 Mw 6.6 Meckering earthquake is one of a series of historical surface rupturing earthquakes (1968 Meckering, 1970 Calingiri, 1979 Cadoux, 2008 Katanning, and 2018 Lake Muir) (Dawson et al., 2008; Gordon and Lewis, 1980; Lewis et al., 1981) hosted within the South-West Seismic Zone (SWSZ) in southern Western Australia (Doyle, 1971). The SWSZ resides predominately within the Yilgarn Craton (*Figure 1*), an assemblage of predominately Archean granitoid-greenstone rocks (Wilde et al., 1996).

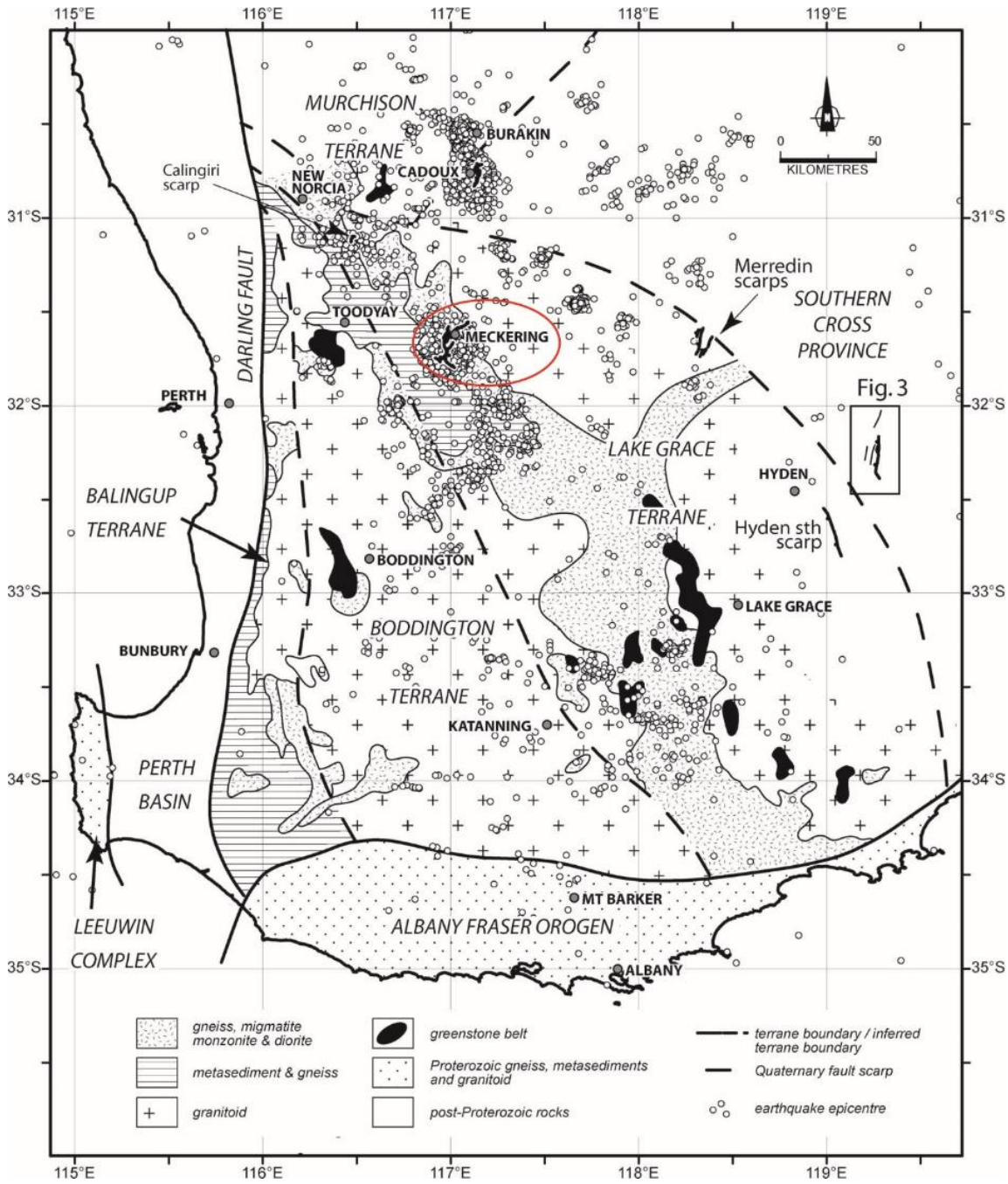

Figure 1: Regional geology surrounding the Meckering earthquake (red circle) and SWSZ seismicity up to 2008: Figure 2 from Clark et al. (2008)

The SWSZ extends roughly NW-SE within a region of the Yilgarn Craton consisting of poly-deformed and metamorphosed crystalline basement (*Figure 1*). The SWSZ extends across three tectono-

stratigraphic terranes; the Boddington Terrane, Lake Grace Terrane and Murchison Terrane (Dentith and Featherstone, 2003; Wilde et al., 1996). Due in part to few basement outcrops, the boundaries between terranes are poorly constrained. Gravity data show that the boundary between the Boddington and Lake Grace Terranes is a major east-dipping geological structure (Clark et al., 2008; Dentith and Featherstone, 2003), interpreted as a large thrust zone based on dating and metamorphic facies analysis across the two terranes (Wilde et al., 1996). Historic seismicity generally aligns with this structure, and occurs on the eastern side of it (Dentith and Featherstone, 2003).

The Meckering and Calingiri events occurred along the edge of the Jimperding Metamorphic Belt within the northern Lake Grace Terrane (*Figure 1*). The Jimperding belt consists of "repeatedly deformed granitoids, gneisses, belts of metasedimentary rocks, small greenstone belts and remnants of layered basic intrusions" (Dentith and Featherstone, 2003).

1.2 Local bedrock

Detailed geological mapping around Meckering identifies small bedrock outcrops of predominately porphyritic or biotite granites, granitic gneiss and micro-monzogranite including in close proximity to surface rupture (Dentith et al., 2009; Lewis, 1969) (See Fig. 5 of Dentith et al. (2009) for detailed map of near-rupture bedrock outcrops). High-resolution aeromagnetic data collected across the Meckering area identified heterogenous bedrock lithology and structure on a local scale (Dentith et al., 2009). Interpretation of this geophysical data highlights two distinct near-vertical structural orientations, NW striking layered rocks consistent with descriptions of the structure and lithology elsewhere in the Jimperding Metamorphic Belt, and SW striking dikes and faults within a granitic area, that overprint the layered rocks. The intersection of these structural grains occurs near the mid-section of the Meckering surface rupture, coincident with the highest recorded vertical displacements (Dentith et al., 2009). *Figure 2* shows publicly available national total magnetic intensity and bouguer gravity anomaly maps. The overall orientations of linear magnetic anomalies identified by Dentith et al. (2009) are visible at the scale of this data, showing the alignment of historic rupture and sets of linear magnetic anomalies. The southern section of rupture is also aligned with a regional gravity anomaly associated with the east-dipping boundary between the Boddington and Lake Grace Terranes.

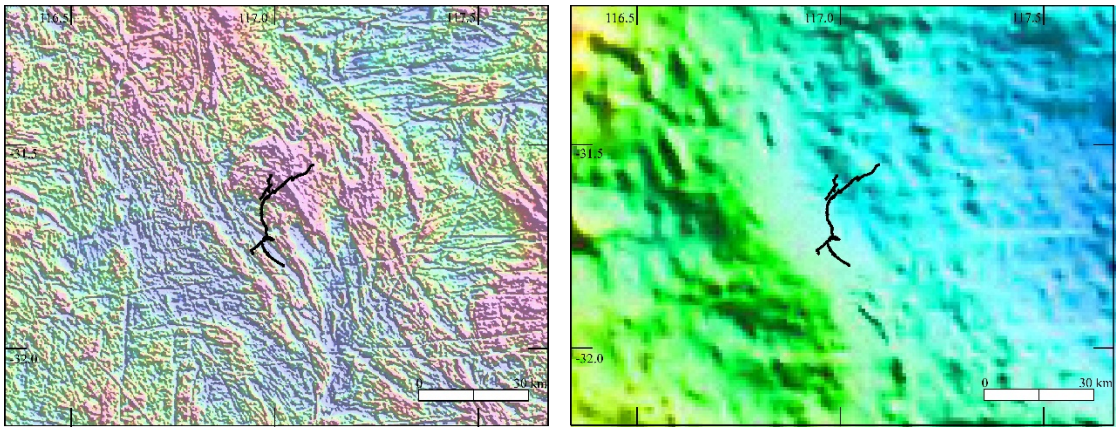

Figure 2: Meckering scarp (black lines) relative to magnetic intensity and bouguer gravity anomaly maps. National bouguer gravity anomaly map: http://pid.geoscience.gov.au/dataset/ga/101104 . *National total magnetic intensity map:* http://pid.geoscience.gov.au/dataset/ga/89596. *Higher resolution magnetic data and interpretation in* Dentith et al. (2009)

1.3 Surficial deposits

Bedrock is overlain with surface deposits of variable thickness including "massive ferricrete, iron-rich pisolitic gravel and aeolian sand and alluvium" (Dentith et al., 2009) (*Figure 3*). A trench dug in 1990

exposed > 2 m of "soil regolith derived from deep weathering of granitic bedrock" (Crone et al., 1997). Clark and Edwards (2018) present two trench logs across the Meckering scarp (originally presented in Clark et al (2011)). One of these excavated across the rupture where it crosses a palaeovalley shows < 2 m of ferricrete and eolian/fluvial/alluvial sands with weakly defined soil profiles. More details are provided in section 4.2.1.

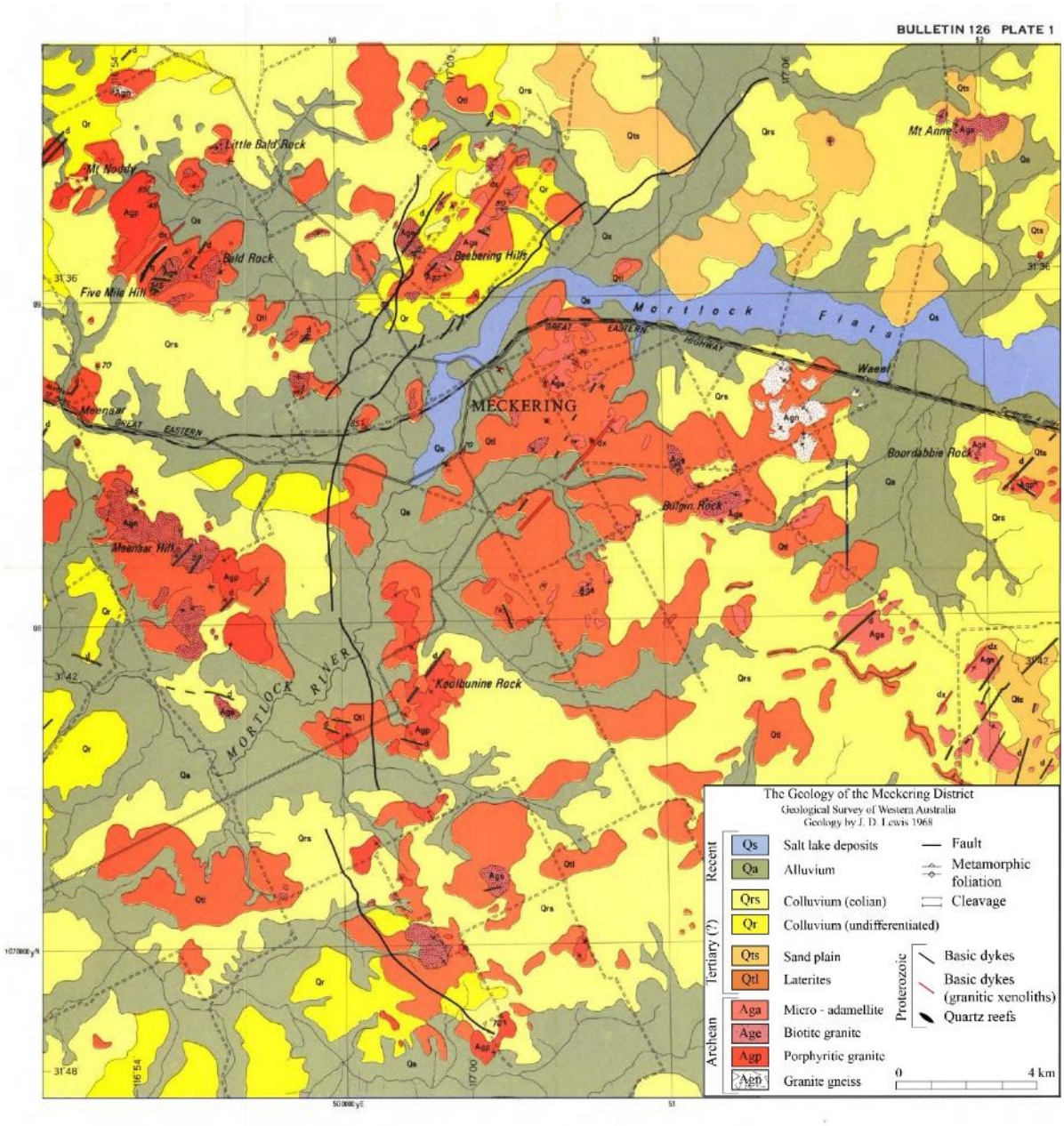

Figure 3: Geological map of basement and surface sediments around the Meckering surface rupture original map by Lewis (1969)*, colourised version reproduced from* Gordon and Lewis (1980) *(legend redrawn from original). Map shows the correlation between bedrock outcrops (e.g. Beebering Hills to the north and Meenaar Hills to the west) with surface rupture orientations.*

2. Seismology

2.1 Epicentre location and magnitude estimates

The Meckering earthquake epicentre was initially located ~ 14 km north of Meckering by the USGS using 13 instruments with an accuracy of ~ 10 km (*Figure 4*). Analysis of four recordings from WA

relocated the epicentre to ~ 3.7 km west of Meckering (Everingham, 1968), which was again relocated ~ 2.5 km NE of Meckering using instrumental recordings from Mundaring geophysical observatory (~ 100 km west of Meckering). The latter is the epicentre contained in the current Geoscience Australia online catalogue and NSHA18 catalogue (Allen et al., 2018). Revised epicentre locations from most agencies fall between the main Meckering scarp and the Splinter scarp. The only published uncertainty comes from Everingham (1968) (± 10 km). All other locations likely have a similar uncertainty (Leonard, 2008), which in most cases means within uncertainty bounds the epicentre could be relocated onto the hanging-wall of the surface rupture.

An isoseismal epicentre was placed in the SE corner of the Meckering township in the middle of the X isoseismal, ~ 4 km west of the surface rupture on the hanging-wall, based on ~ 500 felt reports (Everingham and Gregson, 1970). Vogfjord and Langston (1987) produce best-fitting long-period and short-period synthetic waveforms for a centroid located in the midpoint of the hanging-wall of the Meckering rupture. Clark and Edwards (2018) present a rupture model from an unpublished report which derives an epicentre in the centre of the Meckering scarp hanging-wall. Neither Vogfjord and Langston (1987) or Clark and Edwards (2018) provide coordinates for their epicentre locations, they are shown as approximate locations on *Figure 4*. These epicentres are reproduced in a cross-section in Section 5.1 .

This paper prefers the magnitude (M_W 6.6) of the recently published NSHA18 catalogue (Allen et al., 2018) as they conduct a thorough and consistent reanalysis of Australian magnitude values, particularly to address inconsistencies in the determination of historic magnitude values. Prior to this reanalysis, the magnitude of the Meckering earthquake was reported as 6.9 M_L.

Table 1 : Published epicentre locations, depths and magnitudes

Reference	Agency	Latitude	± (km)	Longitude	± (km)	Depth (km)	M1		M2	
Denham et al (1980)		-31.58		117		5 (Fitch et al 1973)	6.8	Ms		
GA_Online	GA	-31.62		116.98			6.5	Mw	6.9	ML
Everingham (1968)	Mundaring Observatory	-31.62		116.97		7	6.9	ML		
Everingham, et al (1969)	Mundaring Observatory	-31.6		117		<10	6.8	Ms		
Everingham & Gregson (1970)	Mundaring Observatory	-31.62		117		13 ±5; 0 ± 8; 1 ±5	7			
Gordon and Lewis (1980)	Mundaring Observatory	-31.6		117		7	6.9	ML		
Allen et al (2018)		-31.62		116.98		10	6.59	Mw		
Everingham (1968)	USGS	-31.5	10	117	10	0	6	Mb		

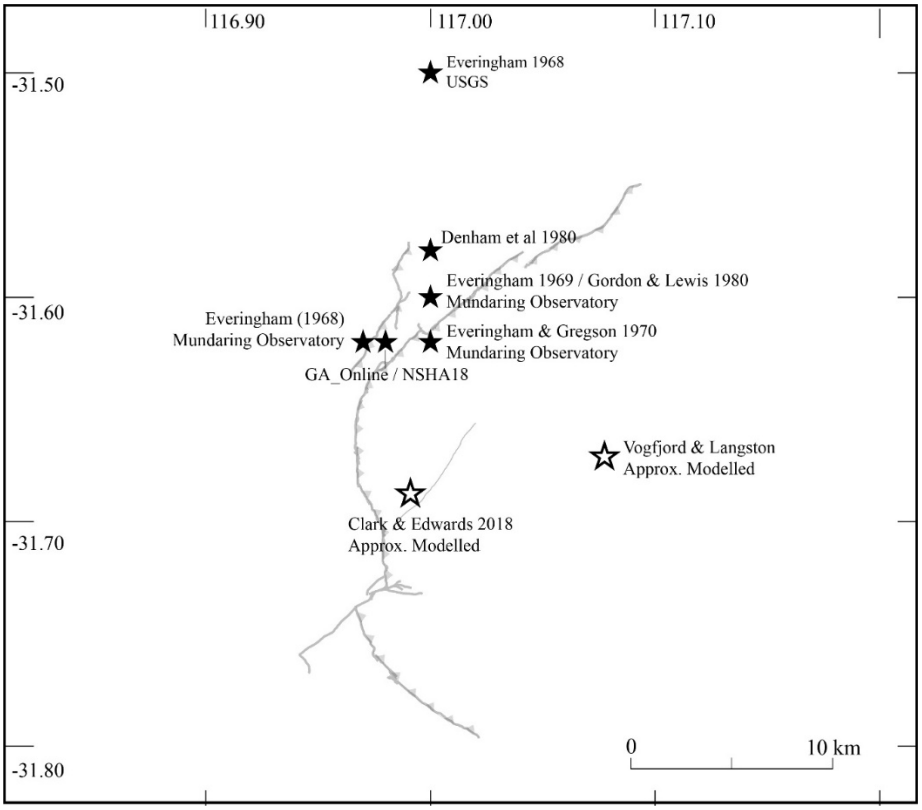

Figure 4: Published epicentre locations around the surface rupture. Open stars show approximate locations of epicentres with no published coordinates, not derived by seismological data

2.2 Focal mechanisms

Four focal mechanisms are published for the Meckering earthquake (*Figure 5*). Fredrich et al. (1988) and Vogfjord and Langston (1987) use moment tensor methods to infer a dominantly reverse mechanism, with N-S striking planes. Both prefer the eastward dipping plane as the fault plane based on the orientation of surface rupture, which shows a slight sinistral component to motion in both mechanisms. Fitch et al. (1973) present a mechanism for the mainshock using p-wave first motions and s-wave polarization from teleseismic data. They note that p-wave data suggest a sub-event initiated 3.5 seconds before the mainshock, and that their solution includes a component of a strike-slip mechanism for this initial event based on p-wave data recorded on instruments within and close to Australia. Leonard et al. (2002) redraw the original Fitch et al. (1973) focal mechanism with a predominately strike-slip sense, using the data presented in Figure 2 of Fitch et al. (1973).

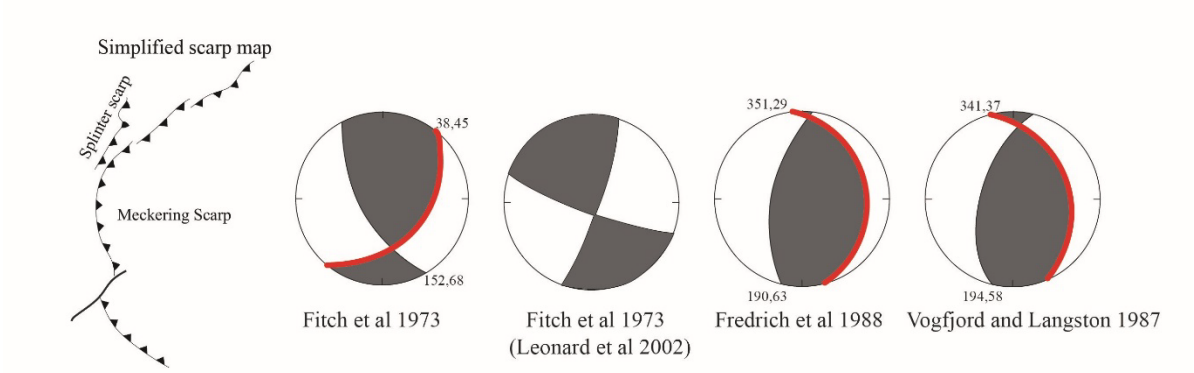

Figure 5: Published focal mechanisms and simplified surface rupture map, digitised from original sources. Preferred plane of the reference publication is shown in red.

2.3 Depth

Hypocentral depth estimates from seismic analysis vary from 1 to 10 km, with Gordon and Lewis (1980) describing initial depths of 0 ± 8 km from the USGS and 7 ± 5 from the Mundaring Observatory (Everingham, 1968). Everingham and Gregson (1970) derive a 13 ± 5 km focal depth based on isoseismal contours. These solutions are too deep to have produced the observed surface rupture, based on seismic moment estimates. The hypocentral depth from a rupture model presented in Clark and Edwards (2018) is roughly 2.5 km based on a 37° dip, with an epicentre in the central area of the Meckering scarp hanging-wall.

Fitch et al. (1973) suggest aftershock locations support a mainshock depth < 10 km (aftershock depths were not presented). Depth estimates of < 10 km were also made based on interpretation of seismic data from four WA stations, 13 USGS stations, and macroseismal intensities (Everingham et al., 1969). Reanalysis of seismic waveform data suggested shallow fore- and aftershock events (1 - 2 km), which were used to support a shallow hypocentre at 1.5 km (Langston, 1987; Vogfjord and Langston, 1987). Body wave inversion methods were used to obtain an optimal centroid of moment release depth of 3 km and a scenario where a fault plane with maximum width 10 km (in the mid-point of the surface rupture) ruptures down to a depth of 6 km (Vogfjord and Langston, 1987). Fredrich et al. (1988) obtain a similar optimal centroid depth of 2.3 km by analysing the interaction of SH and P waveform data.

2.4 Bi/Uni lateral rupture

Vogfjord and Langston (1987) derive source parameters from body wave inversions and use these to model two scenarios of either shallow earthquake initiation and downward propagation of energy, or deeper initiation and upward propagation. They acknowledge that long period waveforms match either model, but they favour a shallow initiation model based on short-period waveform results and interpretation of the crustal setting of the earthquake. They acknowledge that short-period records are not deterministic of exact initiation depth.

Clark and Edwards (2018) present a rupture model from an unpublished report which shows rupture nucleation in the centre of the Meckering scarp hanging-wall, propagating bi-laterally to create slip along the southernmost segment, and shallow slip in the northern segment. Their model incorporates both teleseismic body waves and surface offset measurements along three modelled faults aligned to the arcuate surface rupture.

We propose in this paper a model where rupture initiates on the Splinter fault producing the sub-event which occurred 3.5 sec before the mainshock (Fitch et al., 1973; Fredrich et al., 1988; Vogfjord and Langston, 1987). The Splinter scarp orientation matches well with the Fitch et al. (1973) P-wave first motion focal mechanism. Fredrich et al. (1988) suggest that the P-wave first motion data may describe a change in the fault plane orientation and dip following rupture initiation related to multiple faults rupturing, but discount this as unlikely (with no further discussion provided). We suggest that the data best match a model where rupture initiates on the Splinter fault and propagates upwards to the surface and down to an intersection with the central and/or northern faults of the Meckering fault system, before propagating bi-laterally along all faults within the Meckering system (as defined in Section 3.2) producing the mainshock event.

Fredrich et al. (1988) derive a seismic moment which includes the sub-event and suggest that their total seismic moment is approximately 25 % greater than seismic moment derived by Vogfjord and Langston (1987) who omit the initial sub-event from their calculation. We calculate width of the Splinter Fault (5.6 km) using $W = Mo / \mu DL$ where:

- Mo is the difference of the Fredrich et al. (1988) and Vogfjord and Langston (1987) solutions ($10.4 * 10^{25} – 8.2 * 10^{25}$ dyne/cm = $2.2 * 10^{25}$ dyne/cm);

Note: Fredrich et al. (1988) report their Mo as 10.4 * 10^{18} Nm, but we assume they mean 10.4 * 10^{25} dyne/cm as the reported units convert to an unreasonably low seismic moment. There is some uncertainty in their seismic moment as we could not replicate the reported value with the parameters they provide.

- L (length) is 9 km based on surface rupture length (Section 4.2);
- D is length-weighted average net-slip of 1.34 m (see King et al. (2019) (in review) for details on the derivation of this value);
- μ is shear modulus (shear wave velocity squared x density) based on parameters from Fredrich et al. (1988) (shear wave velocity = 3.4 km s^{-1}, density = 2.8 g cm^{-3}.

We test our model by assuming the Splinter fault meets the Meckering at the base of the derived Splinter fault width (3.8 km). Assuming a planar geometry and applying a preferred dip for the Splinter fault (30° ± 10°) and Meckering central / north faults (40° ± 10°) (based on surface measurements see Section 3.4 and Gordon and Lewis (1980)) produces a depth of intersection at 2.8 km (consistent with centroid depth estimates of 2.3 - 3 km(Fredrich et al., 1988; Vogfjord and Langston, 1987)) at a distance of 3.3 km SE of the Meckering scarp (almost directly underneath the town of Meckering).

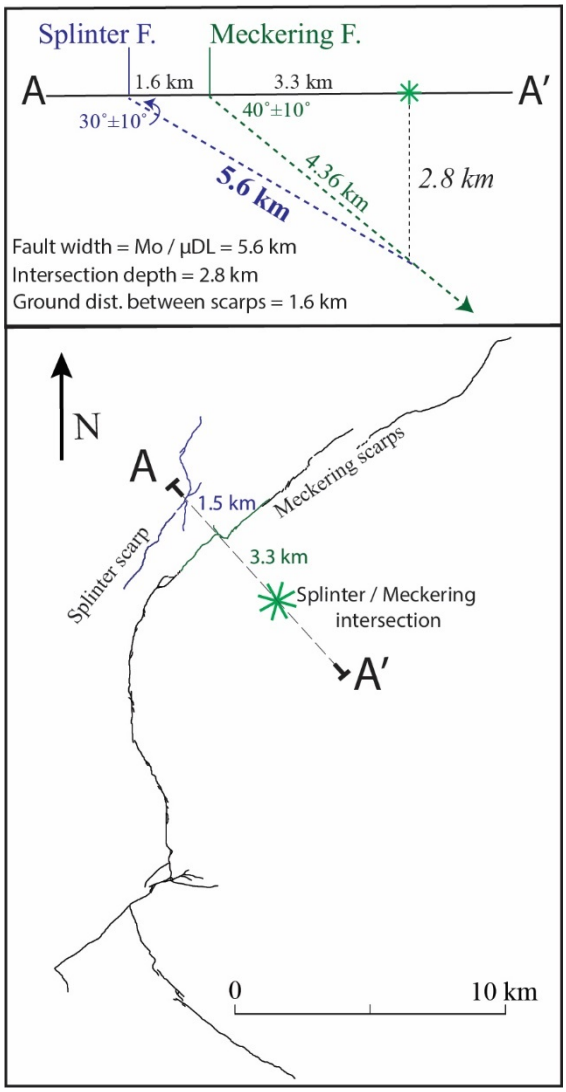

Figure 6: Cross-section showing the derived width of the Splinter fault and preferred dip values for the Splinter and Meckering scarps. Depth and ground distances are calculated based on dip and fault width. The cross section location drawn in plan-view is where the distance between the scarps (1.5 km) best matches the derived ground distance (1.6 km)

We believe that a model were rupture initiates on the Splinter Fault matches well with available data. This model could be refined by reanalysing the original waveform data to improve seismological inputs (e.g. seismic moment), investigating the 3D geometry of fault intersections, conducting finite fault modelling of the sub-event and main-shock, and conducting Coulomb stress modelling to investigate whether an initial rupture on the Splinter fault is consistent with rupture onto the Meckering fault.

2.5 Foreshock / aftershocks

Three events of ~ M_L 3.2 were felt by residents the month prior to the mainshock, while three foreshocks of M_L 3.8, 3.7 and 4.2 were felt within a 1 hr period 11 days prior, causing minor damage to a farm house. Minor shaking was felt on the day of the mainshock, but was considered a normal occurrence for the town (Everingham, 1968; Gordon and Lewis, 1980).

Two temporary seismometers were deployed by the Mundaring Geophysical Observatory immediately following the earthquake (Everingham, 1968; Everingham and Gregson, 1971). Between 1968 and 1976 the observatory published data for 142 aftershocks greater than M_L 2.9, with the largest a M_L 5.7 the day after the mainshock (Everingham and Gregson, 1971; Gordon and Lewis, 1980). Locals reported damage caused by aftershock activity including new surface cracking and damage to shop interiors following small magnitude events unrecorded at the Mundaring Observatory (Gordon and Lewis, 1980). Given the damage described it is assumed these aftershocks were very shallow events (< 1 km).

Original published aftershock data do not contain location uncertainties, and occur on both the east and west sides of the rupture (e.g. on both the hanging-wall and foot-wall). Original data also do not contain depth analysis, though reanalysis of aftershock waveforms using sP-P ratios determined shallow depths (< 2 km) for aftershocks (Langston, 1987). This reanalysis does not map the aftershocks relative to the surface rupture location or geometry. Lewis (1990b) present analysis of a 1990 M_L 5.5 earthquake located close to the rupture trace on the hanging-wall of the Meckering scarp.

3. Surface Rupture

3.1 Authors / map quality

The Meckering fault ruptured predominately across pastoral properties ~134 km from Perth along a main highway. This event was easy to access, and thorough mapping of the rupture was conducted directly onto aerial images during the months following the event (Everingham, 1968; Gordon and Lewis, 1980; Lewis, 1969). The rupture trace was not surveyed along, and only a few cadastral surveyed profiles were completed across the rupture where it offset infrastructure. The highest resolution complete published map of the rupture comes from a comprehensive 250-page report by Gordon and Lewis (1980) (Lewis (1990) provides a 2-page summary of the main report) and is at a 1 : 50 000 scale, with two 1 : 500 detailed maps. The rupture trace from this map is reproduced in the GA Neotectonics Features database (Clark, 2012), and sections of the rupture are visible in Google and Bing satellite imagery, though they do not always align with the digitised rupture due to datum transformation differences.

3.2 Length and shape

The surface rupture was mapped as 3 major faults, the Meckering fault, Splinter Fault and Burges Fault Complex (Gordon, 1971; Gordon and Lewis, 1980). Other minor ‘faults’ include Posterior Fault, Robinson Fault, Anterior Fault, Sudholz Fault and Chordal Fault (Gordon and Lewis, 1980). Later historical Australian surface ruptures were classified as scarps, which avoids confusion between topographic expression of surface deformation and underlying geological structures (or seismological approximations of geological structures). To avoid confusion, we adopt this nomenclature for the Meckering structures mapped as ‘faults’ and refer to them as scarps when describing surface observations.

The 37 km long Meckering Scarp is the surface expression of the main rupture; it has an arcuate shape which is concave relative to the hanging-wall and preferred epicentre location. Authors prior to Gordon and Lewis (1980) variably describe the length as 32 km to 43 km long (Conacher and Murray, 1969; Everingham, 1968; Everingham et al., 1969; Gordon, 1968). The rupture has four 0.3 to 1.5 km wide step-overs separating strands of 6 to 11 km length, with multiple < 300 m steps mapped along its length. The step-overs are all linked by extensional fractures or rupture ramps as mapped on the 1 : 50 000 map (Gordon and Lewis, 1980).

The Splinter scarp is 9 km long and has a 1.5 km wide step-over between linear segment lengths of ~ 1.6 and 4.8 km. It occurs on the foot-wall of the Meckering scarp, ~ 0.4 to 9 km to the NW, and is parallel for some of its length. The Splinter scarp hosts displacements up to 0.67 m and is considered to be a primary rupture by this paper because it shows length, displacement and orientation consistent with primary slip along basement structures proximal to the main scarp. It is not counted in the original 37 km Meckering scarp length (*Figure 7*b).

The 'Burges Fault Complex' is a set of complex ruptures, fractures and fissures comprising the Burges scarp, Robinson scarp, Anterior scarp and Posterior scarp. The Burges scarp and Anterior scarp are 1.8 km and 1.2 km long and run between the biggest step-over in the Meckering scarp trace. These are best described as a network of dense short en-echelon fracture/ramp structures along a semi-linear trend. Together they accommodate vertical displacements up to 0.60 m and are considered primary rupture by this paper. They are not counted in the original 37 km Meckering scarp length (*Figure 7*b).

The Robinson scarp is a ~ 3.7 km long extension of the Burgess scarp onto the foot-wall of the Meckering scarp, and the Posterior scarp is a ~ 2 km long extension onto the hanging-wall. These scarps accommodate minor offset and may better be defined as networks of secondary fractures and fissures.

The "Chordal Fault" and "Sudholz Fault" are hanging-wall features ~ 6.5 km and 4 km long. The Chordal scarp is associated with lateral and normal surface offset, and was only noted by the land owner six weeks after the main rupture. It is interpreted by the Gordon and Lewis (1980) as either aftershock related or a result of hanging-wall settling following the main uplift and is probably better classified as a secondary extensional fracture or fissure. The Sudholz scarp was recognised seven months after the mainshock as a 400 m long series of discontinuous extensional fractures across the Mortlock River. Again, it may be better described as secondary extensional fractures (potentially related to aftershock activity) rather than primary rupture.

Figure 7 shows various measures of length along the Meckering scarp including the length reported by Gordon and Lewis (1980), quoted in subsequent publications (Fig. 7b). This length does not include the Splinter or Burges ruptures, though those two scarps have displacement characteristics of primary ruptures. Including these features shows a length of 45.8 km (Fig. 7c). Figure 7d simplifies ruptures to straight traces and defines distinct faults where mapped primary rupture has gaps/steps > 1 km and/or where strike changes by > 20° for distances > 1 km. This results in five faults being defined, explored in more detail in King et al. (2019) (in review).

Figure 7e presents portions of the scarp where more than two vertical displacement measurements of greater than 0.2 m occur within a distance of 1 km (data from Gordon and Lewis (1980)). Applying cosmogenic erosion rates from lithologically and climatically analogous settings of Australia (0.3 – 5 m/Myr; Bierman and Caffee, 2002) suggests that 0.2 m of scarp height could be removed within 35 – 660 kyrs, leaving 25 km of rupture length (i.e., 25 km of residual surface rupture with relief ≥ 0.2m) visible in the landscape. This suggests that the surface scarp may persist within this landscape as a mappable scarp, and places some constraints on recurrence as no topography from prior rupture is visible in the landscape today. In this calculation we assume that the scarp is shallowly underlain by granitic bedrock and that the scarp erodes more rapidly than the surrounding terrain at rates commensurate with Bierman and Caffee (2002). We do not account for erosion rates of any duricrust

which may overlie granitic bedrock or anthropogenically- and/or climatically-modulated variations in erosion rates.

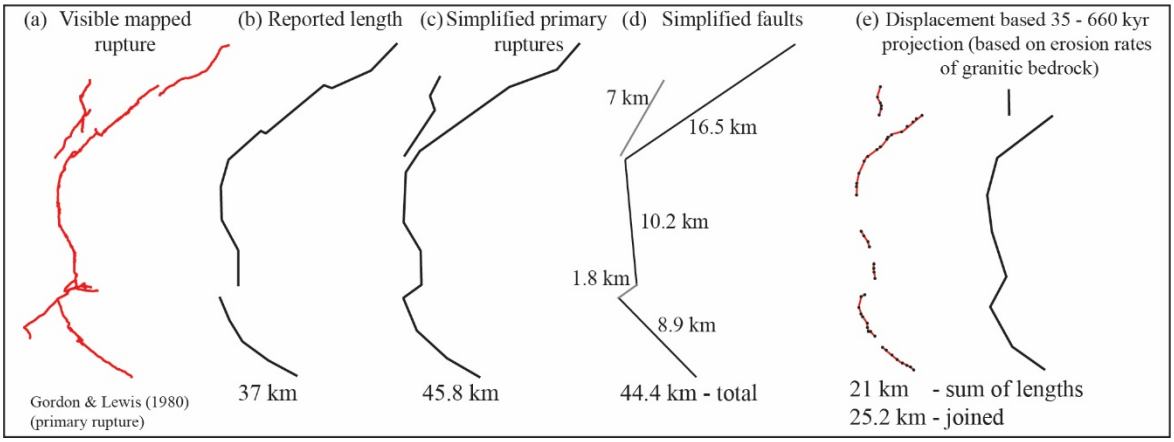

Figure 7: Measures of length for the Meckering surface rupture and underlying faults.

3.3 Scarp strike

The relatively linear northern section of the Meckering scarp has a general strike of 050°, the central section is highly arcuate but has a general trend towards 005°, and the slightly less arcuate southern section has a strike of 320°. The Splinter scarp has an overall strike of 030° (the Meckering scarp strikes towards 045° where the two are coincident with each other). The Burgess scarp complex strikes 045°, with a 40 - 50° inter-scarp angle compared to the strike of the Meckering scarp in this location.

3.4 Dip

Measured dip of the surface rupture is highly variable between 15 – 54° (*Figure 8*) (Gordon and Lewis, 1980). Authors recording dip suggest these variations occur based on type and depth of surficial sediments (Everingham et al., 1969; Gordon and Lewis, 1980). Dip derived based on the calculated slip direction (from measured lateral, vertical and horizontal/heave offset) shows much more confined range of values, averaging 40°. Both sets of data seem to show shallower dips on the southern portion of scarp (~ 20 - 30°), and steeper in the north (~ 40 - 50°). Average dip of the Meckering Scarp has been reported as 35° (Everingham, 1968), 39° (Gordon and Lewis, 1980) and 42° (Lewis, 1990b). The Splinter fault shows a measured dip of 30° and calculated dips of 24 - 41°, with a reported overall dip of 28° (Gordon and Lewis, 1980). The unpublished rupture model presented in Clark and Edwards (2018) uses a three fault model with dip constrained to 37° for each fault plane, possibly derived from the focal mechanism of Vogfjord and Langston (1987), which has a preferred dip of 37°.

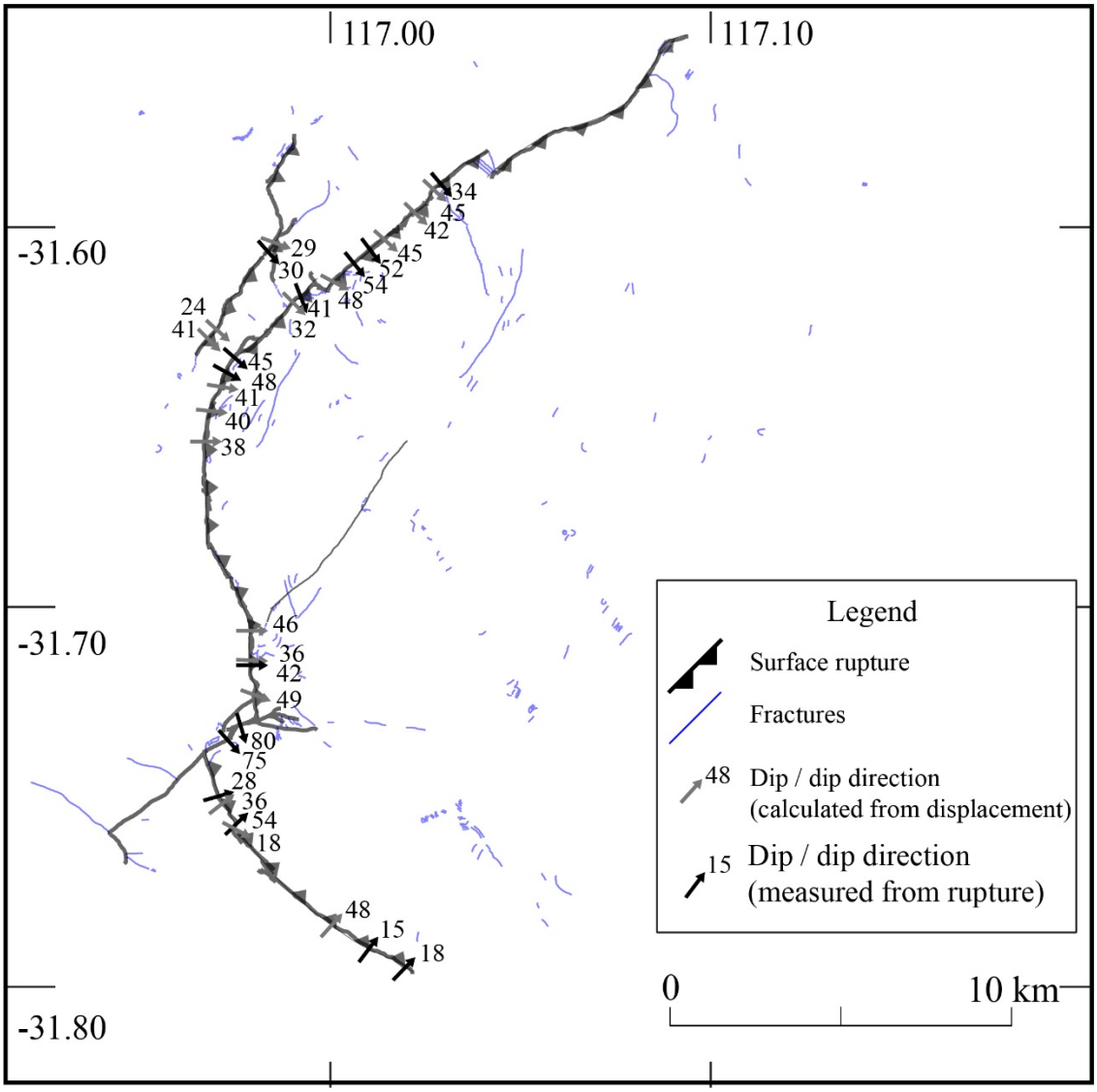

Figure 8: Map of the Meckering scarps, fractures, and dip measurements. Surface data from Gordon and Lewis (1980).

3.5 Morphology

The Meckering scarp has variable morphology including single discrete rupture, duplexing discrete ruptures, back-thrusting, and broad warping of the hanging-wall relative to the foot-wall (e.g. folding at the rupture trace rather than discrete rupture). Authors recognised that these differences in rupture morphology correlate to differences in surficial sediment composition (e.g. sandy river sediments vs. clay-rich ploughed fields) and thickness (e.g. where bedrock was close to the surface) (Conacher and Murray, 1969; Everingham et al., 1969; Gordon and Lewis, 1980). While these changes in morphology along short sections of scarp are explored in detail in the text of Gordon and Lewis (1980), the complexity of rupture morphology is not recorded on the 1 : 50 000 map. Aerial and ground images published in various publications also show significantly more variation to the scarp morphology (e.g. duplexing structures) than is shown on the 1 : 50 000 map, though this complexity is mapped in detail for the Burgess scarp and Meckering town 1 : 500 maps (Gordon and Lewis, 1980). These sections and aerial photos show that discontinuous discrete rupture, duplexing discrete ruptures and small < 50 m wide step-overs were common along the Meckering scarp. Clark and Allen (2018) digitise rupture traces visible in an aerial photograph published in Gordon and Lewis (1980) to compare with modern drone derived imagery (*Figure 12*). They compare the fine scale complexity visible 2-days after the rupture

and how that complexity has changed in the 50 years since rupture (Clark, 2018; Clark and Allen, 2018; Clark and Edwards, 2018).

Step-overs and breaks in the main rupture trace show dense fracture arrays connected discontinuous discrete ruptures, and parallel extensional fractures are common along single strands of discrete rupture. The other mapped scarps are characterised by less discrete rupture and significantly more extensional fracturing, fractures with lateral displacement, and fractures with no evident displacement, generally in linear en-echelon configurations to define the scarp as mapped (Gordon and Lewis, 1980).

3.6 Lateral displacements

Dextral offset of the Meckering scarp was recorded where roads, train tracks, pipelines fences and field furrows crossed the scarp, and from observed slickensides and relative movement of fault segments and fracture networks (Figure 9). The maximum amount of dextral displacement was 1.5 m recorded in the mid-section at the central apex of the curved rupture. The four major stepovers between segments of the Meckering scarp show dextral transtensional offset. The most prominent of these is the Burges scarp area which is composed predominately of dextral en echelon fractures, related to transfer of compression between segments of the Meckering scarp. Warped and bent train tracks that crossed the scarp at an almost perpendicular angle clearly record the dextral movement. Gordon and Lewis (1980) discount 16 of their 20 slickenside measurements as they do not appear to match the sense of movement captured from surveyed displacements across the scarp. They suggest these disparate results result from movement in two stages with pure thrust propagation caused an opening between each side of the surface rupture prior to dextral offset, so dextral slickensides were not be recorded (Gordon and Lewis, 1980). Alternate explanations have not been proposed within the literature.

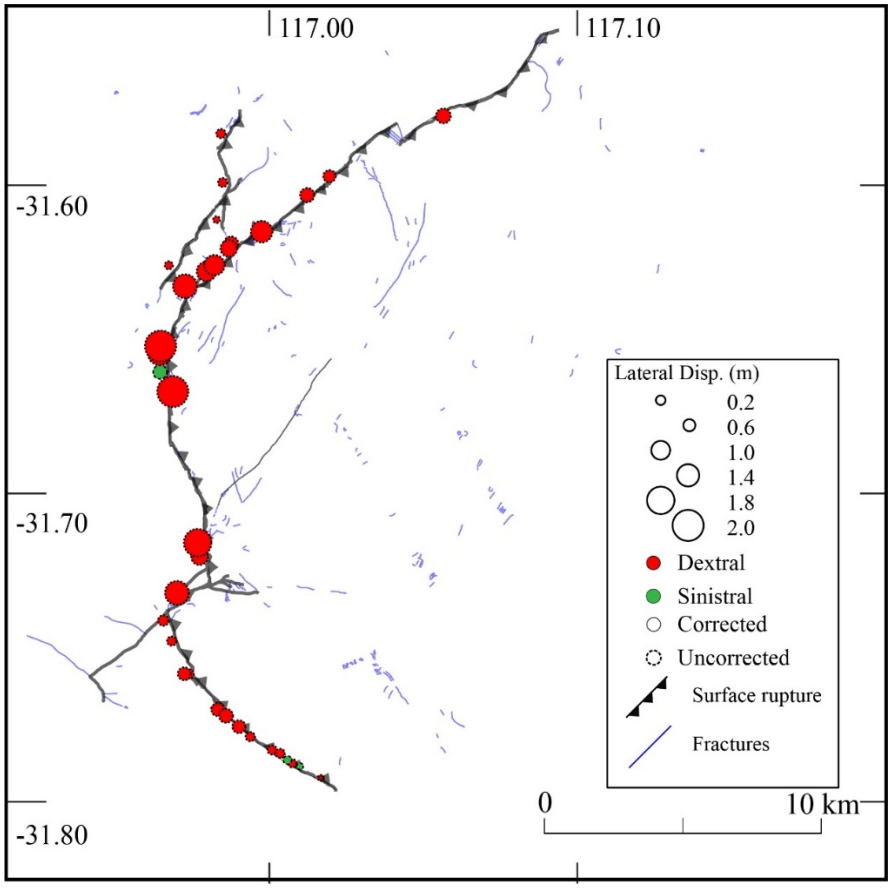

Figure 9: Lateral displacement measurements (data digitised from Gordon and Lewis (1980)). Uncorrected measurements are offsets measured from features (fences, roads, etc) not perpendicular to the strike of surface rupture.

3.7 Displacement

The Western Australia Lands and Surveys Department re-surveyed cadastral boundaries and fences that had been disrupted by faulting providing ten displacement measurements across the scarp (Gordon and Lewis, 1980). The authors do not provide location coordinates for these measurements, though they are shown on the 1 : 50 000 map (digitised for this paper, see Appendix A: Methods). Surveys to re-establish the height of the Great Eastern Highway provide a levelling profile across the Meckering scarp (digitised for this paper, see Appendix A: Methods). A 230 m profile shows 1.43 m extrapolated offset of hanging-wall relative to foot-wall along the highway. There is an additional 0.8 m hanging-wall uplift across a 20 m distance attributed to hanging-wall folding. This profile also shows a ~ 10 cm depression on the hanging-wall ~ 10 km east of the rupture, a feature that coincides with a 4 km wide zone of extensional fractures between the northern and southern fault tips shown in the 1 : 50 000 map and labelled the Backscarp Zone by Gordon and Lewis (1980). The seemingly linear trend of fractures across the hanging-wall in *Figure 11* are due to fracture observations being made along roads.

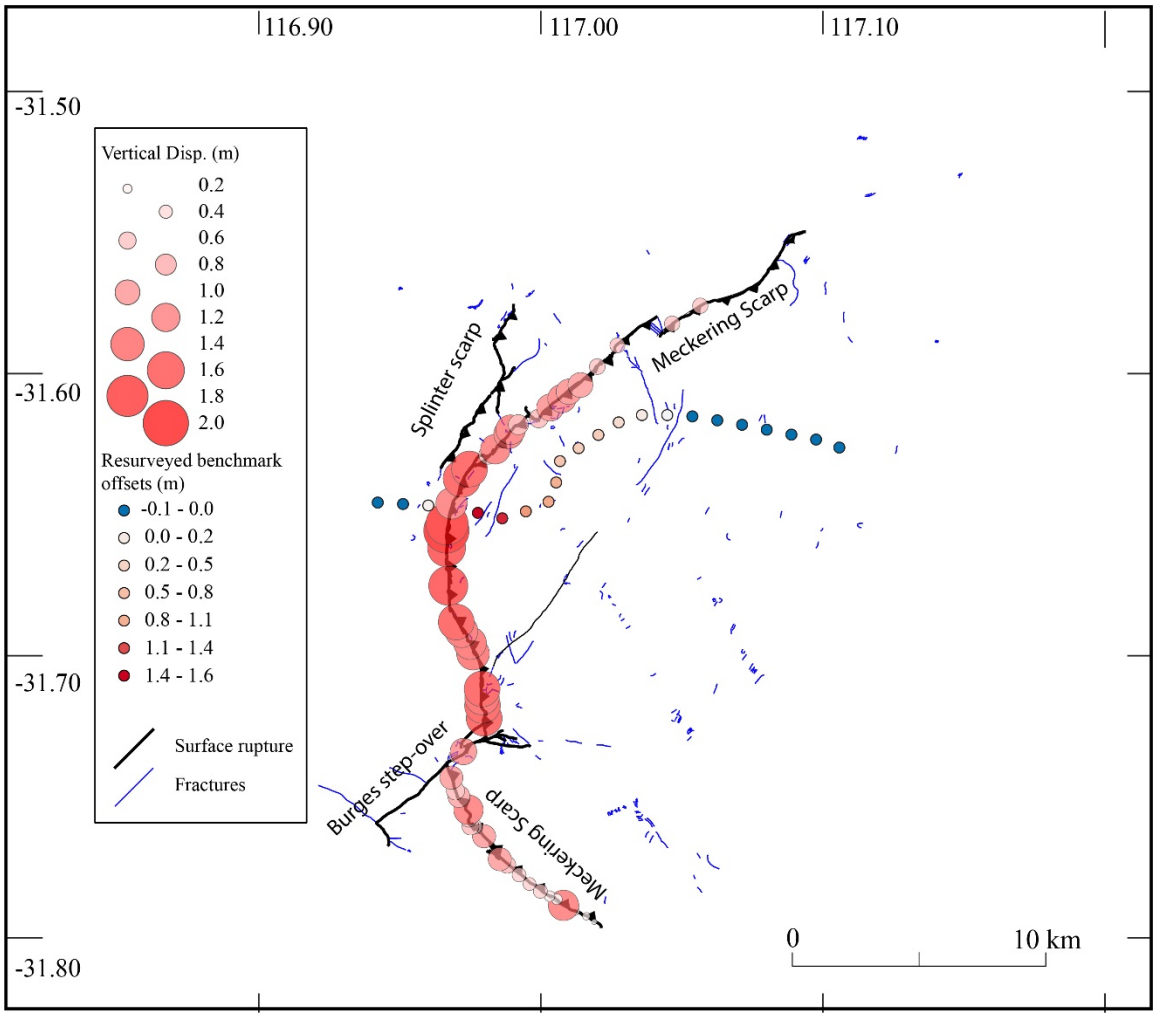

Figure 10: displacement data along and across the Meckering scarp. Data digitised from Gordon and Lewis (1980)

Vertical displacement measured at displaced fence lines (tables 10 - 11 Gordon and Lewis (1980), digitised for this paper) show a slightly asymmetrical along-fault displacement envelope. Displacement values are at a maximum in the central parts of the rupture and diminish where rupture curvature changes from N-S trending, to the NE-SW and SE-NW trending limbs. Displacements south of the Burgess step-over are almost 50% lower on average than those north of this feature (0.59 m and 1.21 m respectively). The displacement envelope for the foot-wall Splinter scarp show maximum

displacements along a 1.5 km NW-SE trending step-over of the predominately NE-SW trending scarp, close to where the cross section in *Figure 6* is drawn.

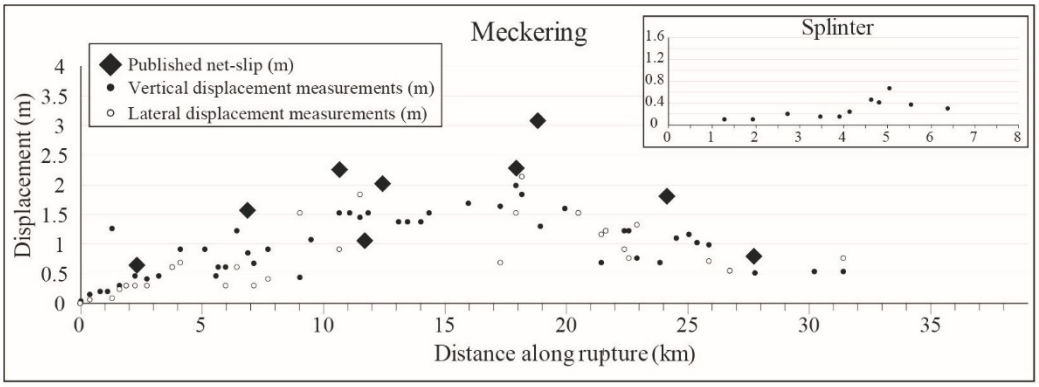

Figure 11: Vertical displacement measurements along the Meckering and Splinter scarps, digitised from (Gordon and Lewis, 1980). (See Appendix A: Methods).

3.8 Environmental damage

Environmental damage is described by Gordon and Lewis (1980) and includes surface rupture, fractures/cracking and fissures, landslides and rock falls, sand-blows, and hydrological anomalies. The length and offset of the Meckering scarp fits the ESI-07 scale classification X, which also fits descriptions of fissures developed along the rupture. Some fractures/cracks have lengths and widths as described by ESI VIII, but most are better characterised as ESI VI-VII.

Several small landslides were reported along road cuttings and gulleys in Perth (~ 140 km) and south of Cunderdin (~ 25 km), and small rockfalls were reported along rail cuttings in Avon Valley (~ 100 km) (Gordon and Lewis, 1980). Given a lack of information regarding these events, we assign them ESI IV based on the number of reports and estimated susceptibility of these environments to mass movements. A cave system at Yanchep 127 km west of Meckering also reported damage to stalactite formations, with two caves closed due to the damage (Gordon and Lewis, 1980). Several small sand blows were recorded on the hanging-wall associated with salt-flats of the Mortlock River and groundwater flows adjacent to railway tracks (Gordon and Lewis, 1980). We assign these to ESI V based on descriptions in Serva et al. (2016). Three bore records from around Perth recorded the earthquake as a vertical displacement of water height (Everingham and Parkes, 1971; Gordon, 1970; Gordon and Lewis, 1980; Gregson et al., 1972), we assign these an ESI IV. Multiple authors note the lack of damage to large trees within a few kilometres and along the rupture (Everingham, 1968; Everingham et al., 1969) and no shaking related vegetation damage could be seen in any published photographs. Dead grass can be seen along the rupture in multiple photographs, associated with root tear.

Gordon and Lewis (1980) document small ‘slumps’ which occur in proximity to extensional features (e.g. the Chordal scarp on the hanging-wall) and seem to relate to internal gravitational collapse from circular or arcuate extensional fractures (they may be similar to ‘polygonal cracking’ described in Fig 6. King et al. (2018). Gordon and Lewis (1980) describe fractures identified near the 1970 Calingiri rupture ~ 100 km NE that appeared infilled and many years old, which they suggest may relate to the 1968 Meckering earthquake, though the evidence is circumstantial and unverified.

Gordon (1968) and later authors describe ~ 1.5 m vertical offset of the Mortlock River where it crosses the fault, raising potential flood levels for Meckering township by 12 cm (Gordon and Lewis, 1980). This and four other small offset drainages were cleared following the earthquake to prevent future flooding events (Gordon and Lewis, 1980). Clark and Edwards (2018) (*Figure 12*) present a comparison between rupture trace visible in a 1968 aerial photograph, and the trace visible in 2018 drone derived

imagery which shows significant foot-wall ponding and sedimentation where the stream was offset. This geomorphic change is also visible on Bing and Google satellite imagery. High resolution UAV derived elevation models show the previous and new position of the tributary (Clark and Edwards, 2018).

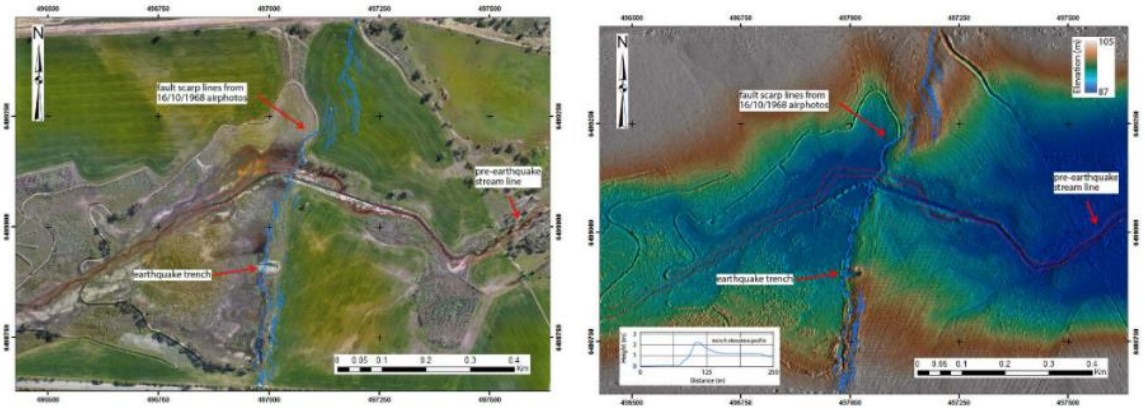

Figure 12: Geomorphic changes across an offset Mortlock River tributary captured 50 years after the Meckering earthquake from figure 16 Clark and Edwards (2018) (also the location of trench one as described below).

4. Paleoseismology

4.1 Authors / mapping / quality

No detailed palaeoseismic studies have been published specifically on the Meckering rupture, though Clark et al. (2011) and Clark and Edwards (2018) present data from two trenches crossing the rupture. The original rupture mapping of Gordon and Lewis (1980) was conducted prior to palaeoseismic techniques such as trenching becoming common procedure. Crone et al. (1997) mention a 2 - 3 m deep trench dug in 1990 for a intraplate earthquake symposium field trip (Gregson, 1990), but no logs of this trench are published.

4.2 Trenching

4.2.1. Identified units

Crone et al. (1997) note > 2 m of soil regolith in the trench exposed in 1990, with the only identifiable structural features related to the 1968 rupture. Clark et al. (2011) present two trench logs, the first across the rupture where it offset a stream close to the Great Eastern Highway and the second in an area of maximum vertical offset on an upper slope of farmland. The first trench was ~ 3 m deep and composed of fluvial and alluvial sands of various thicknesses and lithological properties, this trench did not expose bedrock. A weakly developed soil horizon is noted ~ 0.1 - 1m below the surface, overlain by a sandy topsoil with abundant root traces. The second trench exposed altered granitic bedrock at 1 - 1.5 m depth, overlain by sediments including ~ 1 m of ferricrete and < 0.5 m of sand (Clark et al., 2011). Clark and Edwards (2018) suggest that fractures/shear bands in the ferricrete which do not reach the surface may relate to 1968 rupture or to a prior event.

Clark et al. (2011) also include data from an unpublished report related to trenches across two sand dykes in the vicinity of those described in Gordon and Lewis (1980). This study found potential evidence of two generations of liquefaction, though they may also relate to root casts. More details of the unpublished data are provided in Clark and Edwards (2018), describing grainsize fining away from the 'vent' and silt accumulations along the vent margin. The authors note that these features are common in liquefaction-induced sand dykes, though the features superficially resemble root-casts (Clark and Edwards, 2018).

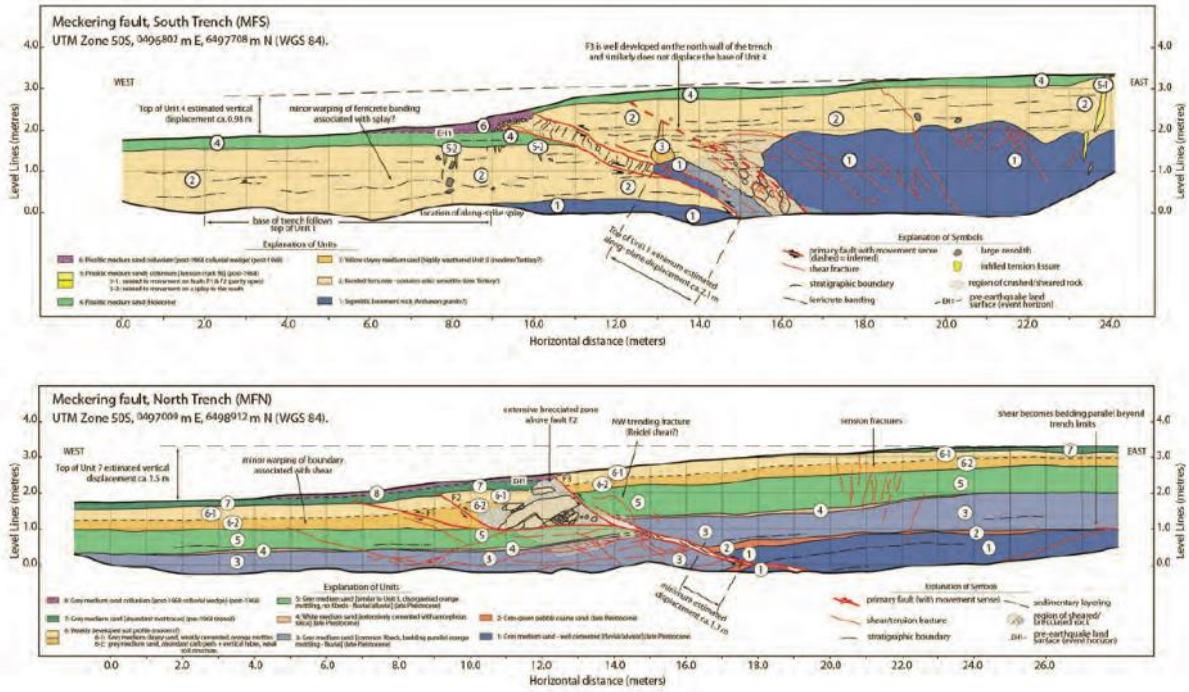

Figure 13: Trench logs from unpublished study, included in (Clark et al., 2011), Clark and Edwards (2018) and Clark (2018)

4.2.2. Structural interpretations

Structures exposed in the first trench shows historic displacement along three primary rupture strands, with multiple tension fractures on the hanging-wall, and some minor warping of buried sediments on the foot-wall (*Figure 13*). Displacement in the second trench was concentrated in a single narrow band, associated with a single discrete rupture at this location. Conjugate fractures are mapped in the bedrock on the hanging-wall, with one fracture extending to the surface and infill of an extensional fissure extending down to basement level. Some of the identified historical fracturing only occurs in the basement and does not reach to surface level.

4.3 Topography

Several authors note that the Mortlock River changes from westerly flow to south-west flow quite abruptly ~ 2 km from the Meckering rupture and flows roughly parallel to the rupture for ~ 10 km before crossing the rupture (in the central region where offset is near-maximum) and continuing SW (Gordon and Lewis, 1980; Lewis, 1969). The morphology and flow of the river also changes from a shallow wide diffuse river bed with salt pans along its length, to a narrower deeper 'rejuvenated' river channel. Yilgarn craton rivers to the north and south of the Mortlock river show similar changes in morphology and direction, recognised as a major drainage change within the Swan-Avon System (Jutson, 1934; Mulcahy, 1967) and attributed to Eocene uplift along the Darling Fault (Beard, 1999; Jakica et al., 2011; Salama, 1997).

Clark and Edwards (2018) explore the relationship between the historic rupture, potential prior seismic offset of the Mortlock River, bedrock/geophysical controls on river morphology/direction, and larger scale drainage patterns. They include a high-resolution drone derived DEM across where the Morlock River crosses the Meckering scarp. They find no link between river morphology/direction and prior rupture, and no evidence in the Quaternary floodplain for prior Quaternary rupture.

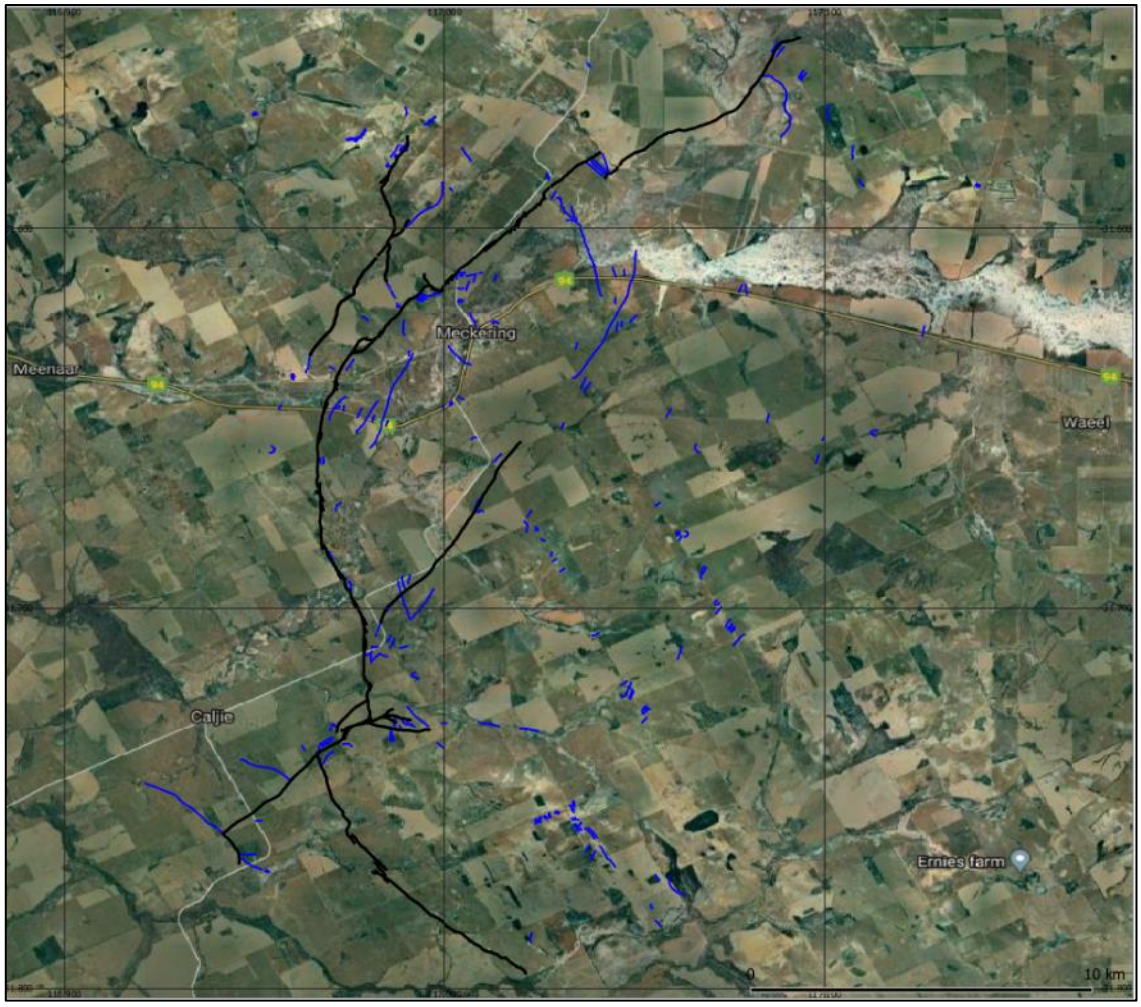

Figure 14: Google Earth satellite imagery showing the association of the Mortlock East river and Meckering scarp and fractures (©2019 CNES / Airbus, Map Data, Google)

4.4 Other

Possible liquefaction features (e.g., two generations of sand-filled features that may be root casts or sand dykes) were identified in trenches excavated proximal to the Meckering (Clark et al., 2011; Clark and Edwards, 2018). Two OSL results are presented in Clark et al. (2011) taken above (~ 0.5 m) and below (~ 0.8 m) one of the sand dykes identified on the hanging-wall of the 1968 rupture. These bracket the sand feature between 17 - 20 ka. The second sand feature overlies the sedimentary layer dated at 17 ka, giving an age bracket of 0.15 – 17 ka. These features, if seismically induced, are considered unrelated to prior rupture along the Meckering scarp as trenching shows only historic offsets. The OSL ages do give some constraint on sand accumulation between 0.03 – 0.1 m/kyr.

If induced by liquefaction, these features provide preliminary evidence for strong ground motion intensities at this site that exceeded thresholds for liquefaction triggering. Typical minimum peak ground acceleration thresholds for liquefaction initiation in highly susceptible sediments are 0.1 to 0.15 g (e.g. Quigley (2013)). Using craton-specific ground motion prediction equations (Somerville and Ni, 2010), possible maximum Joyner-Boore distances for scenario earthquakes that could have generated sufficient PGAs to initiate liquefaction at this site are M_w 5.5 (≤ 15 to 30 km), M_w 6.5 (≤ 37 to 60 km) and M_w 7.5 (≤ 100 to 150 km). Clark and Edwards (2018) suggest that sediments in the SWSZ may have been more susceptible to liquefaction prior to agricultural clearing and increasing induration of sediments from salinification. Further research is required to determine whether an earthquake origin is

the most plausible interpretation for these features, and whether they may be of use for future palaeoseismic studies in the area (Clark et al., 2011).

4.5 Slip rate

No strong evidence exists to support rupture along the Meckering scarp between 1968 and the Pliocene(?) formation of ferruginous duricrusts developed in granite on hilltops (Clark et al., 2011; Clark and Edwards, 2018). Recurrence on the underlying faults therefore cannot be demonstrated. The complexity of the scarp does not favour recurrent slip as displacement of intersections between the NE and NW trending basement structures/lithological trends would tend to form a barrier to further slip (e.g. Talwani (1988)). If, instead of on the faults that ruptured in 1968, recurrent slip is accommodated on proximal structure, low bedrock erosion rates (< 5 m/Ma (Belton et al., 2004)) provides an upper constraint for relief generation rates (e.g. *Figure 7*e).

5. Summary

5.1 Surface rupture relationship to Geology

Detailed mapping of the Meckering area was conducted following the earthquake to investigate geological relationships to the rupture (Lewis, 1969), the author found no relationship between rupture orientation and granite foliation but an occasional correlation between rupture and nearby dike orientations. Gordon and Lewis (1980) note that bedrock granite outcrops at the surface as an almost continuous line on the hanging-wall of the rupture, including a westward step of outcrop distribution around the location of the Burgess fault stepover in the Meckering scarp (*Figure 2*, *Figure 3*). They also note that outcrops on the western side are generally more highly weathered.

Dentith et al. (2009) conducted high resolution geophysical mapping across the area and present strong evidence to suggest the location and direction of the Meckering rupture was controlled by basement structures, including NW trending folds and foliation, and SW trending dike systems. Several granitic gneiss basement outcrops exist proximal to the Meckering rupture with foliation orientations aligned with geophysical basement structures, and mapped mafic dykes have a predominately SW trend (Lewis, 1969).

Gordon and Lewis (1980) describe quartz fragments common at the surface along 6 km of the southern section of scarp, and in at least one location the scarp is coincident with a brecciated quartz outcrop (seen in either a creek cutting, or a hole dug across the scarp). They also describe iron-rich soil that post-dates a quartz breccia identified 8 km SW of Meckering, close to the 1968 rupture. They interpret these two observations to suggest the Meckering rupture occurred along a pre-existing ancient fault. Dentith et al. (2009) interpret the basement structure along this southern section as folded stratigraphy, and rupture may have propagated along a lithological boundary.

5.2 Surface rupture relationship to Seismology

The early faulting models developed to describe the seismological and surface data are dated, relative to current understanding of fault rupture. Gordon (1968) describe faulting related to an elevated dome block, Everingham (1968) describes “chipping…on a large scale” and conchoidal fracture, Conacher and Murray (1969) suggest that rain had saturated the soil and it “deformed plastically” along the rupture and Gordon and Lewis (1980) invoke a complicated model related to the arcuate nature of rupture to describe the Meckering fault as a portion of a saucer shaped ‘mobile block’.

A number of publications present fault rupture models more consistent with current theories and models for fault rupture. Denham et al. (1980) propose that pore-water perturbations may have been able to trigger an earthquake on a weathered fault plane, consistent with mechanisms of fluid assisted seismicity (e.g. Balfour et al. (2015)). Dentith et al. (2009) use high-resolution aeromagnetic data to provide a model of failure based on intersecting NE-SW and SE-NW bedrock structures with a central

N-S trending linking structure. Vogfjord and Langston (1987) use a similar three-plane fault model to model long and short period synthetic waveforms. They find this three-fault model fits the long period data well but does not reproduce the observed short period data. Clark and Edwards (2018) present data from an unpublished report which uses a three-fault model to derive a finite rupture model from surface offset measurements and teleseismic body waves.

As discussed in Section 2.4, this paper prefers a model where rupture initiates on the Splinter fault, producing a sub-event matching the observed P-wave first motion data, and propagating onto the Meckering faults to produce the observed mainshock data. Fault geometry based on surface rupture measurements (and assuming planar faults) produces a fault intersection at 2.8 km, consistent with available estimates of centroid depth at 2.3 - 3 km (Fredrich et al., 1988; Vogfjord and Langston, 1987).

The number of distinct faults that are hypothesized to have ruptured in this earthquake (n=4, or n=8 if including the Splinter fault), based on the criteria stated herein, is the highest estimate of multi-fault earthquakes at this magnitude as ascertained from a recent global compilation (Figure 15) (Quigley et al., 2017).

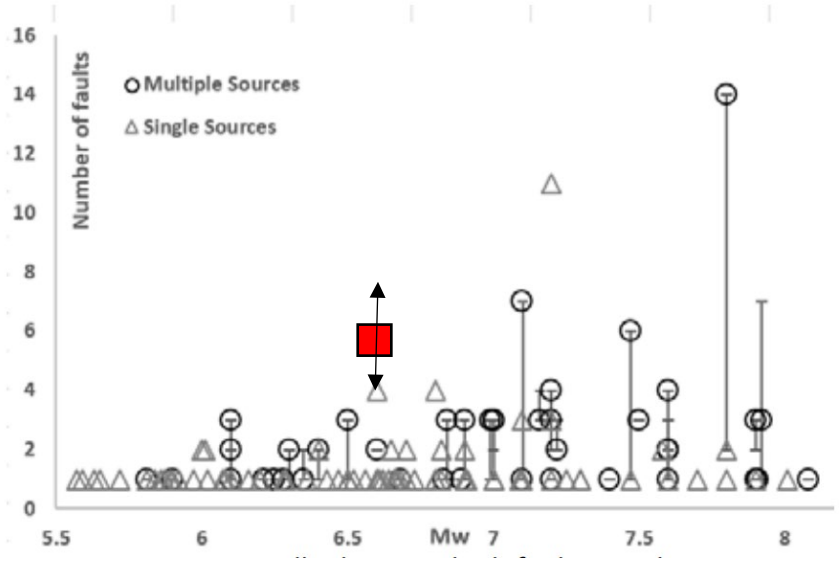

Figure 15: From Fig. 5 of Quigley et al. (2017), Meckering earthquake (red box) plotted against recent global compilation of number of geometrically-distinguished fault ruptures vs. Mw.

Acknowledgements

This research was funded by the Australian Research Council through Discovery Grant #DP170103350. T. King received funding through the Australian Government Research Training Program Scholarship. We would like to acknowledge the Ballardong of the Noongar people of south-west Western Australia as the traditional custodians of the land on which this surface rupture occurred, and where the data described in this paper were collected. The authors declare no conflict of interest.

6. References

Allen, T., Leonard, M., Ghasemi, H., Gibson, G., 2018. The 2018 National Seismic Hazard Assesment: Earthquake epicentre catalogue (GA Record 2018/30). Geoscience Australia, Commonwealth of Australia, Canberra, ACT. https://doi.org/http://dx.doi.org/10.11636/Record.2018.030

Balfour, N.J., Cummins, P.R., Pilia, S., Love, D., 2015. Localization of intraplate deformation through fluid-assisted faulting in the lower-crust: The Flinders Ranges, South Australia. Tectonophysics

655, 97–106. https://doi.org/10.1016/j.tecto.2015.05.014

Beard, J.S., 1999. Evolution of the river systems of the south-west drainage division, Western Australia. J. R. Soc. West. Aust. 82, 147–164.

Belton, D.X., Brown, R.W., Kohn, B.P., Fink, D., Farley, K.A., 2004. Quantitative resolution of the debate over antiquity of the central Australian landscape: Implications for the tectonic and geomorphic stability of cratonic interiors. Earth Planet. Sci. Lett. 219, 21–34. https://doi.org/10.1016/S0012-821X(03)00705-2

Bierman, P.R., Caffee, M.W., 2002. Cosmogenic exposure and erosion history of Australian bedrock landforms. Bull. Geol. Soc. Am. 114, 787–803. https://doi.org/10.1130/0016-7606(2002)114<0787:CEAEHO>2.0.CO;2

Clark, D., 2018. What have we learned in the 50 years since the 1968 Meckering earthquake ? Geoscience Australia, Commonwealth of Australia, Canberra, Australia. https://doi.org/http://pid.geoscience.gov.au/dataset/ga/123342

Clark, D., 2012. Neotectonic Features Database. Geoscience Australia, Commonwealth of Australia, Canberra, Australia.

Clark, D., Allen, T., 2018. What have we learnt regarding cratonic earthquakes in the fifty years since Meckering ? Proc. Aust. Earthq. Eng. Soc. Conf. 2018, Nov 16-18, Perth, WA.

Clark, D., Dentith, M., Wyrwoll, K.-H., Yanchou, L., Dent, V.F., Featherstone, W.E., 2008. The Hyden fault scarp, Western Australia: paleoseismic evidence for repeated Quaternary displacement in an intracratonic setting. Aust. J. Earth Sci. 55, 379–395. https://doi.org/10.1080/08120090701769498

Clark, D., Edwards, M., 2018. 50th anniversary of the 14th October 1968 Mw 6.5 (Ms 6.8) Meckering earthquake (GA Record 2018/39). Geoscience Australia, Commonwealth of Australia, Canberra, ACT. https://doi.org/http://dx.doi.org/10.11636/Record.2018.039

Clark, D., Mcpherson, A., Collins, C., 2011. Australia's seismogenic neotectonic record: a case for heterogeneous intraplate deformation (GA Record 2011/11). Geoscience Australia, Commonwealth of Australia, Canberra, Australia. https://doi.org/http://pid.geoscience.gov.au/dataset/ga/70288

Conacher, A.J., Murray, I.D., 1969. The Meckering earthquake, Western Australia, 14 October 1968. Aust. Geogr. 11, 179–184. https://doi.org/10.1080/00049186908702551

Crone, A.J., Machette, M.N., Bowman, J.R., 1997. Episodic nature of earthquake activity in stable continental regions revealed by palaeoseismicity studies of Australian and North American quaternary faults. Aust. J. Earth Sci. 44, 203–214. https://doi.org/10.1080/08120099708728304

Dawson, J., Cummins, P.R., Tregoning, P., Leonard, M., 2008. Shallow intraplate earthquakes in Western Australia observed by Interferometric Synthetic Aperture Radar. J. Geophys. Res. Solid Earth 113, 1–19. https://doi.org/10.1029/2008JB005807

Denham, D., Alexander, L.G., Worotnicki, G., 1980. The stress field near the sites of the Meckering (1968) and Calingiri (1970) earthquakes, Western Australia. Tectonophysics 67, 283–317. https://doi.org/https://doi.org/10.1016/0040-1951(80)90271-1

Dentith, M., Clark, D., Featherstone, W.E., 2009. Aeromagnetic mapping of Precambrian geological structures that controlled the 1968 Meckering earthquake (Ms 6.8): Implications for intraplate seismicity in Western Australia. Tectonophysics 475, 544–553. https://doi.org/10.1016/j.tecto.2009.07.001

Dentith, M., Featherstone, W.E., 2003. Controls on intra-plate seismicity in southwestern Australia. Tectonophysics 376, 167–184. https://doi.org/10.1016/j.tecto.2003.10.002

Doyle, H.A., 1971. Seismicity and structure in Australia. Bull. R. Soc. New Zeal. 9.

Everingham, I.B., 1968. Preliminary Report on the 14 October 1968 Earthquake at Meckering, Western Australia (BMR Record 1968/142), 1968/142. ed. Canberra, ACT. https://doi.org/http://pid.geoscience.gov.au/dataset/ga/12254

Everingham, I.B., Gregson, P.J., 1971. Mundaring Geophysical Observatory, Annual Report, 1968 (BMR Record 1971/12). Bureau of Mineral Resources, Geology and Geophysics, Canberra, Australia. https://doi.org/http://pid.geoscience.gov.au/dataset/ga/12549

Everingham, I.B., Gregson, P.J., 1970. Meckering earthquake intensities and notes on earthquake risk for Western Australia (BMR Report 1970/97). Canberra, ACT. https://doi.org/http://pid.geoscience.gov.au/dataset/ga/12510

Everingham, I.B., Gregson, P.J., Doyle, H.A., 1969. Thrust Fault Scarp in the Western Australian Shield. Nature 223, 701–703.

Everingham, I.B., Parkes, A., 1971. Intensity Data for Earthquakes at Landor (17 June 1969) and Calingiri (10 March 1970) and their Relationship to Previous Western Australian Observations (BMR Recrod 1971/80), 1971/80. ed. Bureau of Mineral Resources, Geology and Geophysics, Canberra, Australia. https://doi.org/http://pid.geoscience.gov.au/dataset/ga/12617

Fitch, T.J., Worthington, M.H., Everingham, I.B., 1973. Mechanisms of Australian earthquakes and contemporary stress in the Indian ocean plate. Earth Planet. Sci. Lett. 18, 345–356. https://doi.org/10.1016/0012-821X(73)90075-7

Fredrich, J., Mccaffrey, R., Denham, D., 1988. Source parameters of seven large Australian earthquakes determined by body waveform inversion. Geophys. J. 95, 1–13. https://doi.org/https://doi.org/10.1111/j.1365-246X.1988.tb00446.x

Gordon, F.R., 1971. Faulting during the earthquake at Meckering, Western Australia: 14 October 1968. R. Soc. New Zeal. Bulletin 9, 85–93.

Gordon, F.R., 1970. Water level changes preceding the Meckering, Western Australia, earthquake of October 14, 1968. Bull. Seismol. Soc. Am. 60, 1739–1740.

Gordon, F.R., 1968. Reconstruction of Meckering town, a geological appraisal (GSWA Record 1968/14). Geological Survey of Western Australia, Perth, Western Australia.

Gordon, F.R., Lewis, J.D., 1980. The Meckering and Calingiri earthquakes October 1968 and March 1970, Geological Survey of Western Australia Bulletin. Perth.

Gregson, P.J. (Ed.), 1990. Recent intraplate seismicity studies symposium, Perth, Western Australia September 1990 (BMR Record 1990/44). Bureau of Mineral Resources, Geology and Geophysics, Canberra, ACT. https://doi.org/http://pid.geoscience.gov.au/dataset/ga/14335

Gregson, P.J., McCue, K., Smith, R.S., 1972. An explanation of water level changes preceding the Meckering earthquake of 14 October 1968 (BMR Record 1972/101). Canberra, Australia. https://doi.org/http://pid.geoscience.gov.au/dataset/ga/12782

Jakica, S., Quigley, M.C., Sandiford, M., Clark, D., Fifield, L.K., Alimanovic, A., 2011. Geomorphic and cosmogenic nuclide constraints on escarpment evolution in an intraplate setting, Darling Escarpment, Western Australia. Earth Surf. Process. Landforms 36, 449–459. https://doi.org/10.1002/esp.2058

Jutson, J.T., 1934. The physiography (geomorphology) of Western Australia (Bulletin No. 95), Second Edi. ed. Geological Survey of Western Australia, Perth, Western Australia.

King, T.R., Quigley, M.C., Clark, D., 2019. Surface-rupturing historical earthquakes in Australia and their environmental effects: new insights from re-analyses of observational data. Geosciences.

King, T.R., Quigley, M.C., Clark, D., 2018. Earthquake environmental effects produced by the Mw 6.1, 20th May 2016 Petermann earthquake, Australia. Tectonophysics 747–748, 357–372. https://doi.org/10.1016/j.tecto.2018.10.010

Langston, C.A., 1987. Depth of Faulting during the 1968 Meckering, Australia, earthquake sequence determined from waveform analysis of local seismogram. J. Geophys. Res. 92, 11561–11574. https://doi.org/10.1029/JB092iB11p11561

Leonard, M., 2008. One hundred years of earthquake recording in Australia. Bull. Seismol. Soc. Am. 98, 1458–1470. https://doi.org/10.1785/0120050193

Leonard, M., Ripper, I.D., Yue, L., 2002. Australian earthquake fault plane solutions (GA Record 2002/019), 2002/19. ed. Canberra, ACT. https://doi.org/http://pid.geoscience.gov.au/dataset/ga/37302

Lewis, J.D., 1990a. The Meckering earthquake of 17 January 1990 (GSWA Record 1990/6). Geological Survey of Western Australia, Perth, Western Australia.

Lewis, J.D., 1990b. Meckering revisited, in: Recent Intraplate Seismicity Studies Symposium, Perth Western Australia (BMR Record 1990/44). https://doi.org/http://pid.geoscience.gov.au/dataset/ga/14335

Lewis, J.D., 1969. The geology of the country around Meckering (GSWA Record 1969/18). Geological Survey of Western Australia, Perth, Western Australia.

Lewis, J.D., Daetwyler, N.A., Bunting, J.A., Montcrieff, J.S., 1981. The Cadoux Earthqauke (GSWA Report 11). Perth, Australia.

Mulcahy, M.J., 1967. Landscapes, Laterites and Soils in Southwestern Australia, in: Jennings, J.N., Mabbutt, J.A. (Eds.), Landform Studies from Australian and New Zealand. Australian National University Press, Canberra.

Quigley, M.C., 2013. Earthquake clustering, complex fault ruptures, and the geological record.

Quigley, M.C., Mohammadi, H., Duffy, B.G., 2017. Multi-fault earthquakes with kinematic and geometric rupture complexity : how common ? INQUA Focus Group Earthquake Geology and Seismic Hazards.

Salama, R.B., 1997. Geomorphology, geology and palaeohydrology of the broad alluvial valleys of the Salt River System, Western Australia. Aust. J. Earth Sci. 44, 751–765. https://doi.org/10.1080/08120099708728352

Serva, L., Vittori, E., Comerci, V., Esposito, E., Guerrieri, L., Michetti, A.M., Mohammadioun, B., Mohammadioun, G.C., Porfido, S., Tatevossian, R.E., 2016. Earthquake Hazard and the Environmental Seismic Intensity (ESI) Scale. Pure Appl. Geophys. 173, 1479–1515. https://doi.org/10.1007/s00024-015-1177-8

Somerville, P., Ni, S., 2010. Contrast in Seismic Wave Propagation and Ground Motion Models between Cratonic and Other Regions of Australia, in: Proceedings of the Australian Earthquake Engineering Society 2010 Conference, Perth, Western Australia. Perth, Western Australia.

Talwani, P., 1988. The intersection model for intraplate earthquakes. Seismol. Res. Lett. 59, 305–310. https://doi.org/https://doi.org/10.1785/gssrl.59.4.305

Vogfjord, K.S., Langston, C.A., 1987. The Meckering earthquake of 14 October 1968: A possible downward propagating rupture. Bull. Seismol. Soc. Am. 77, 1558–1578.

Wilde, S.A., Middleton, M.F., Evans, B.J., 1996. Terrane accretion in the southwestern Yilgarn Craton: evidence from a deep seismic crustal profile. Precambrian Res. 78, 179–196. https://doi.org/10.1016/0301-9268(95)00077-1

Appendix A: Methods

Digitising vertical and lateral displacement data and benchmark data

The locations of vertical and lateral displacement data collected by Gordon and Lewis (1980) by measuring offset fences, farm furrows, tracks, etc, are shown on Figure 39 of that document. The figure was georeferenced against the digitised fault scarp, points were created at all locations and extracted as a CSV file with x-y coordinates. The location numbers and associated vertical displacement are published in Table 10 of Gordon and Lewis (1980). These were extracted from a pdf into excel, and thoroughly checked for copy errors in the data. Location numbers from the GIS process were cross referenced to location numbers in Table 10, to attach x-y coordinates to each offset measurement. These were imported to GIS. A simplified fault trace was created for the Meckering and Splinter scarps, and a short script[1] was used in QGIS attribute manager field calculator to extract the distance of each vertical offset measurement along the simplified fault trace. The shape file was again extracted into a final CSV with x-y coordinates, vertical offset measurements, and distance along fault data.

Offset benchmark data are not published in a table, but appear as graphs in Figures 69 and 70 of Gordon and Lewis (1980), with the x-axis being distance along the Great Eastern Highway between Northam-Meckering-Cunderdin. Centimetre grids were drawn across the graphs in Adobe Illustrator, and x-y data were read off into a CSV file. The national road network shape file was used to extract the Great Eastern Highway between Northam-Meckering-Cunderdin and QGIS's "points along lines" was used to extract points at 1 km intervals. These data were extracted as a CSV with x-y coordinates, and matched against the X axis read from the graphs in Figures 69-70 of Gordon and Lewis (1980). The data were then reimported to QGIS to create a shapefile showing offset of benchmarks as measured and shown graphically in Gordon and Lewis (1980).

Digitising dip data

Dip measurements were digitised from a georeferenced version of Plate 2 of Gordon and Lewis (1980) which presents both measured dips (from trenches, holes across the scarp, exposed rupture planes) and calculated (from displacements). Dip data were collected as attributes in a line shapefile (with the line drawn along the strike of the rupture at the measurement location). Strike values were extracted from lines using a short script[2] and the shapefile was converted into points using "points along lines" (GDAL process in QGIS). Points were extracted into a CSV file with x-y coordinates. Dip directions were calculated in the CSV file.

[1] line_locate_point(geometry:=geometry(get_feature('Line', 'id', '1')), point:=$geometry)

[2] Case when yat(-1)-yat(0) < 0 or yat(-1)-yat(0) > 0 then (atan((xat(-1)-xat(0))/(yat(-1)-yat(0)))) * 180/3.14159 + (180 * (((yat(-1)-yat(0)) < 0) + (((xat(-1)-xat(0)) < 0 AND (yat(-1) - yat(0)) >0)*2))) when ((yat(-1)-yat(0)) = 0 and (xat(-1) - xat(0)) >0) then 90 when ((yat(-1)-yat(0)) = 0 and (xat(-1) - xat(0)) <0) then 270 end